System identification & uncertainty quantification using orthogonal excitations & the Semi-span SuperSonic Transport (S^4T) model

Jennifer Heeg[1] and Carol D. Wieseman[2]
NASA Langley Research Center, Hampton VA 23681

Orthogonal harmonic multisine excitations were utilized in a wind tunnel test and in simulation of the SemiSpan Supersonic Transport model to assess aeroservoelastic characteristics. Fundamental issues associated with analyzing sinusoidal signals were examined, including spectral leakage, excitation truncation, and uncertainties on frequency response functions and mean-square coherence. Simulation allowed for evaluation of these issues relative to a truth model, while wind tunnel data introduced real-world implementation issues.

Nomenclature

f	=	frequency variable, (Hz)
f_{MS}	=	frequencies contained in the multisine excitation, (Hz)
n	=	number of segments, ensembles, in a Fourier coefficient calculation
nf	=	number of frequency components contained in a single multisine excitation
$nfft$	=	Fourier analysis block size, (samples)
ni	=	number of orthogonal multisine signals in an excitation set
$samp$	=	sample rate (samples/sec)
$\breve{u}_i$	=	sinusoidal component of multisine signal
$u_j(t)$	=	multisine signal
α	=	statistical significance level
γ^2_{xy}	=	mean square coherence between an input, x, and an output, y
σ	=	standard deviation
ω	=	frequency variable, (radians)
AEI	=	Aerodynamic Efficiency Improvement
CPE	=	Controller Performance Evaluation
CSD	=	Cross-spectral density function
DFT	=	Discrete Fourier Transform
FRF	=	Frequency Response Function
G	=	Open loop plant frequency response function
HT	=	Horizontal Tail
JWS	=	Joined Wing Sensorcraft
MIMO	=	Multi-Input Multi-Output
NIBAFTZ	=	nacelle inboard aft vertical accelerometer
PSD	=	Power Spectral Density function
P_{xx}	=	PSD of the input, x
P_{yy}	=	PSD of the output, y
S^4T	=	Semi-span SuperSonic Transport
^	=	approximate quantity based on a data sample

[1] Research Engineer, Aeroelasticity Branch, Mail Stop 340, Senior Member AIAA.
[2] Research Engineer, Aeroelasticity Branch, Mail Stop 340, Associate Fellow AIAA.

I. Introduction

NASA's Subsonic Fixed Wing project has a principal technical goal to innovate techniques to produce reduced-weight aircraft with increased functionality. The vision for accomplishing this goal is multidisciplinary, with an approach based on the functional system rather than on a material component or a structural layout. While both of these latter aspects contribute strongly to developing a lightweight aircraft system, the approach being taken is to design the vehicle around its mission. The long-range vision includes highly-distributed control effectors within a structure designed to respond to the efforts. The desired responsiveness of the structural system drives the concept to a flexible vehicle that includes utilizing significant aeroservoelastic effects. This approach requires testing and evaluation of systems that have multiple- simultaneously active- control paths. The current paper continues the research to develop and apply test methods that will facilitate evaluation of such systems.

A method for optimal multiple input design for evaluating stability and control parameters has been developed and applied in flight.[1] This method involves superposition of harmonic sinusoids with frequency content in the range of the dynamics of interest and phase optimization to minimize peak-to-peak amplitudes. The approach is of interest here because it can be used to generate excitation signals that are simultaneously applied to multiple control effectors and produce responses which are separable according to the contribution of the individual control effectors. This approach is accomplished by determining the Fourier transform frequency content that is resolvable within the excitation time length and distributing that frequency content among the control effectors. Multiple excitation signals which are orthogonal in both the time and frequency domains can be generated based on the frequency parsing of harmonic sinusoids, which may then be applied simultaneously to the set of multiple control effectors.

Prior work[2] extended the range of application of this established excitation methodology to an aeroelastic problem. Testing and evaluation of sets of orthogonal multisine signals were applied to the Aerodynamic Efficiency Improvement (AEI) Joined Wing Sensorcraft (JWS) wind tunnel model, described in references 3, 4 and 5. This initial evaluation of the methodology required adapting the methodology to include a significantly larger frequency range for the excitation than that typically required for stability and control parameters estimation. The increase in frequency range is not readily traded for decreasing the resolution of the frequency range because resolving aeroelastic modal characteristics demands more dense frequency spacing than steady or quasi-steady aerodynamic quantities. This demand leads to a significant increase in the number of sinusoidal harmonics which are required to comprise a single multisine excitation. Other potentially suitable excitation sets have been developed; reference 6 summarizes benefits and drawbacks to numerous types.

The current paper shows results obtained by applying the multisine excitation method to the Semi-Span SuperSonic Transport (S^4T) wind-tunnel and simulation models.[7,8,9] Under the auspices of the Fundamental Aeronautics Program, the simulation models were developed and four wind tunnel tests were conducted in the NASA Langley Transonic Dynamics Tunnel. Two objectives of the first two wind-tunnel tests were to understand the wind-tunnel model and to develop state-space representations of the wind-tunnel model for use in subsequent control law design. A primary objective of the final two wind-tunnel tests was to assess the performance of numerous control laws designed for ride quality augmentation, gust load alleviation and flutter suppression.

The remainder of this paper is organized as follows. The objectives and approach are first discussed. Then, background material is presented including specifics of multisine signal sets, the testbed, analysis methods utilized, and an assessment of standard selections of processing parameters. Data from the wind tunnel test is briefly presented to motivate the need to examine information in simulation. Results from analyzing simulation data are then discussed. Lessons learned from the simulation data are then applied to the wind tunnel data.

II. Objectives & Approach

The objectives of the current work are to investigate the sources of uncertainties in the open and closed loop system aeroservoelastic responses. In this study, we focus on frequency response function (FRF) estimates. The approach is to obtain an accurate estimate of the FRF from the data, and understand and quantify the variation and uncertainties on the FRF estimates. The specific sources of variation examined in this work include processing parameter choices, simultaneous excitation, and extraction from closed loop system data.

Before these specific sources of variation can be addressed, however, a fundamental understanding of the processing of this special class of data has to be gained. These fundamentals are examined in this current work; much of the groundwork was laid by analyzing sinusoidal information, although it is not presented here. Multisine signals are linear combinations of sine waves and the extensions of the lessons learned through simple test case analysis were applied to multisine data sets. There is added complexity in the processing of multisine information relative to random excitation data. This complexity has been cited as a reason that the methodology is sparingly

used, though promising in terms of enhanced results and improved test utilization. Schoukens etal[10] offer a promising solution to this obstacle using resampling and smoothing.

III. Multisine excitation signals

A multisine signal is composed by adding sine wave time histories. Each multisine signal is a sum of harmonic sinusoid components with frequency content unique relative to the other multisine signals in the orthogonal set. The frequency content of each multisine signal and the power at each frequency are chosen so that applying each signal to a different input of the system can adequately excite the system dynamics over the frequency range of interest. The frequencies used in constructing the multisine component sine waves, f_i, are calculated as integer multiples of the fundamental frequency, f_0, of the excitation time length specified. These frequencies are identical to the frequencies used in computing the discrete Fourier transform (DFT) of a signal of this same time length. Phase of each component, φ_i, is randomly assigned, drawn from a uniform distribution. The equation for each sine wave component is given by (1).

$$\breve{u}_i(t) = A_i * \sin(2\,\pi\, f_i\, t + \varphi_i) \quad \textbf{(1)}$$

The number of multisine signals, ni, determines the spacing of the frequency content. In the JWS testing, as many as 13 orthogonal multisine signals were required. In the S^{4}T case, 2 orthogonal signals are utilized. Each multisine signal is created by summing the component sine waves, Eq. (2). The amplitude, Ai, was determined by a user-controllable amplitude level, K, and by uniform power across all frequencies. Uniform power over all frequencies requires that the power to any given frequency be inversely proportional to the number of frequencies in that signal, n_f, (2).

$$A = K * Power = K * \sqrt{\frac{1}{n_f}} \quad \textbf{(2)}$$

$$u_j(t) = \sum_{i=j}^{ni} \breve{u}_{((i-1)*ni+j)}(t) \quad \textbf{(3)}$$

For the S^{4}T test, only one set of multisine excitations were used. They were designed with an excitation time length and multisine signal period of 105 seconds. This distinction of excitation time length and multisine signal period is being made explicitly to convey the idea that perhaps they should not be equal. The possibilities in data processing options will revisit this idea later in this paper. The time length of the multisine signal period sets the finest possible frequency resolution as 0.0095 Hz. Two signals are required, so this resolution must be at least halved. The choice was made to skip every second frequency, making the final frequency resolution or spacing within each orthogonal signal 0.0381 Hz. The desired frequency range was 1 to 35 Hz. Dividing this frequency range, 34 Hz, by the frequency spacing, 0.0381 Hz, produces the number of sinusoids that are summed to produce each orthogonal multisine signal. The signals were thus each composed of 893 sinusoids. A segment of each of the excitations is shown in Figure 1.

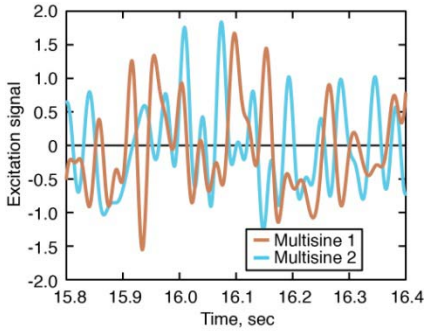

Figure 1 Multisine excitation signals

IV. Wind tunnel model

Previous efforts, utilizing the Aerodynamic Efficiency Improvement (AEI) Joined Wing SensorCraft (JWS) model, produced research questions that the S^4T is more properly suited to address. The JWS model provided the testbed for initial aeroelastic investigations using multisine excitations. In the primary test configuration, a control law was required to actively trim the model. There was no provision for performing open loop and closed loop testing with the same boundary conditions- a major obstacle in assessing the goodness of open loop plant results extracted from closed loop system information.

Comparison of extracted open loop plant characteristics with a truth model acquired from direct measurements of open loop system responses was the primary driver for utilizing the S^4T configuration. Figure 2 shows an illustration of S^4T model including instrumentation. The S^4T model is a sidewall mounted semi-span configuration with 3 control surfaces. The aileron and the horizontal tail were both utilized during the current investigation. Although there were numerous sensors available, most of the control law that were designed and tested utilized the nacelle inboard aft vertical accelerometer (NIBAFTZ) as the feedback parameter.

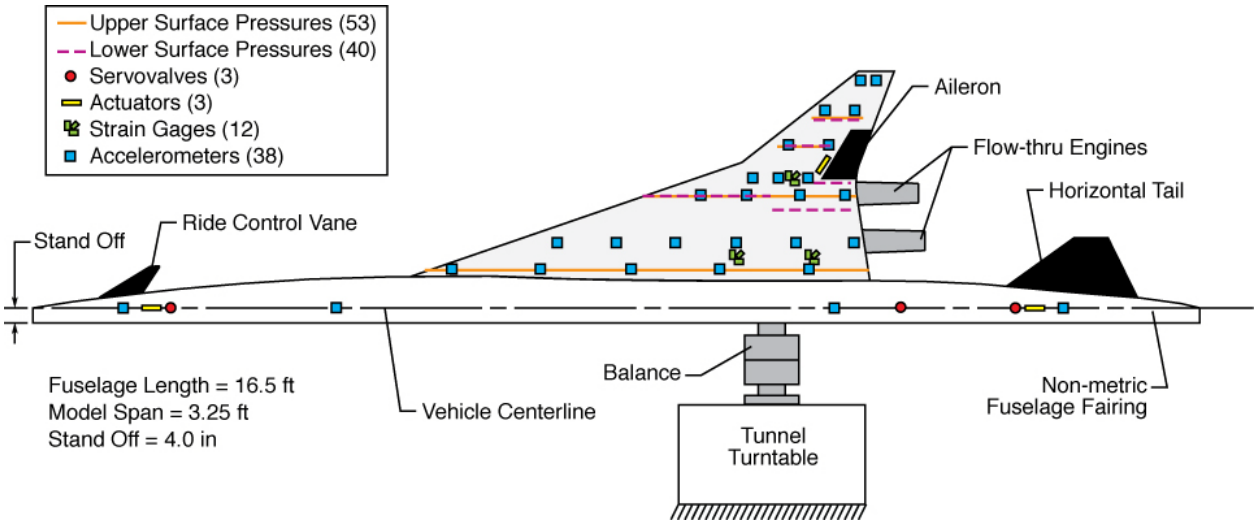

Figure 2. SemiSpan SuperSonic Transport model; instrumentation & layout

V. Analysis methods

Fourier analysis[11,12] is used throughout this work. Specifically, the discrete Fourier transform (DFT) is employed to compute Fourier representations of finite-length signals. The DFT is a finite length sequence rather than a continuous variable. Its values correspond to samples, equally spaced in frequency, of the Fourier transform of a signal. The Power Spectral Density (PSD) function is calculated from the Fourier coefficients, as is the Cross-Spectral Density (CSD) function. In the current work, ensemble or segment averaging is used to compute estimates of the PSD and the CSD. These ensemble averages are then used in computing the Frequency Response Functions (FRFs) and mean-square coherence, γ^2_{xy}, referred to in this paper as the coherence or coherence function.

The controller performance evaluation (CPE) method was developed and demonstrated in the wind tunnel environment in references 13, 14, and 15. The CPE method is used in the current work to extract the open loop plant from the closed loop system excitation data. The CPE method accounts for the presence of the feedback loop, while direct plant extraction methods require assumption that the inputs to the open loop plant are orthogonal to each other. With the current signals, the excitations are orthogonal, but the open loop plant inputs are nonorthogonal due to the effects of the control law feedback. That is, the feedback signals have components which are correlated to each of the excitations that are present. The CPE method works by decomposing the output signals and the feedback signals into the orthogonal components produced by each of the orthogonal excitations.

If a single-input-single-output control law is used, and the only excitation is applied to the feedback control effector, direct plant extraction is a better technique to use than CPE, as it contains the uncertainties associated with

only 1 frequency response function calculation. Utilizing the CPE process involves evaluation of 2 frequency response functions.

Open loop and closed loop CPE data sets were obtained using simultaneous multisine excitations. When Multi-Input-Multi-Output (MIMO) controllers are evaluated, both the horizontal tail (HT) and the aileron are excited. Figure 3 shows the basic block diagram of the feedback system. Definition of the excitation, command, and control law output signals are shown in the Figure 3.

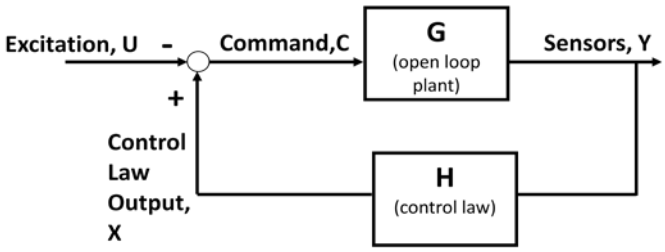

Figure 3 Block diagram of feedback system

VI. Assessment of real-time analyses parameters performed in near-real time

Wind tunnel test data was acquired using orthogonal multisine excitations. The frequency response functions were utilized to predict open and closed loop stability, as well as comparison data for modifying simulation models. The goodness of the predicted aeroelastic characteristics and simulation model updates is directly a function of the goodness of the computed frequency response functions.

During testing, the FRFs were computed in near-real-time to provide on-line predictions to provide recommendations for proceeding with the testing. In this processing, it was typical to utilize overlap averaging of subsets of the data and to window those blocks with a function that tapers at the ends. During the S^4T testing, it was typical to use a block size of 2^12 (4096) points, windowed with a Hanning window, and overlapping adjacent segments by 75%.[16] The resulting FRFs and the subsequent predictions exhibited a good deal of variation, as mentioned in reference 16. The root cause of the variation could lie in the experimental itself, or it could lie in the processing of the data. The experimental data was generated by exciting the system at specific frequencies through the use of the multisine excitations. There are 0 frequencies in common between the set applicable to a window of 4096 samples and the multisine signals that were generated to fit into a 105 second window at 1000 samples/second. This mismatch in frequencies is a potential cause of spectral leakage that is investigated here as one of the potential causes of the variation.

A concern in performing this type of experiment is the signal to noise ratio. In the case of a turbulent wind tunnel, the turbulence is a powerful excitation source. In conducting a flutter test of an aeroelastic model, there is always a tightrope being walked between having enough excitation to get a reasonable measurement, and perturbing the model into an unstable state.

A statistical analysis of the open loop data without excitation compared to the open loop data with excitations showed that the standard deviations of the accelerometer responses increased less than 10% with the multisine excitation applied. Responses from strain gauges showed only a 1% increase with the multisine excitations applied. The S^4T team recognized the most responsive sensors, however, and control law designs focused on using the most responsive to the control effector excitations relative to the tunnel turbulence. In this paper, only the chosen control feedback sensors are examined. For simplicity, most of the results shown in this paper are for a single sensor, the nacelle inboard aft vertical accelerometer, NIBAFTZ.

VII. Baseline analysis of wind tunnel data

As a starting point, the analysis parameter set used for on-line data processing of the S^4T testing was examined. For the current research effort, we changed both the window shape and the overlap percentage of the Fourier analysis segments. Throughout this paper, the analyses performed use a rectangular window. This is following the recommendation of Harris[17], as well as detailed analyses of pure sinusoids.

The overlap used in segmenting the data for ensemble of block averaging to compute the PSDs and CSDs was generally set to a large value to obtain more averages. While several references have demonstrated that the results

obtained using a Hanning window cease to improve for overlaps greater than 67%, no such demonstration was found in the literature regarding the rectangular window.[18] Previous analysis of multisine signals for the JWS and an example found in literature[19] showed that continued improvement is gained for overlap values above 90%. The results shown in this paper have 95% overlap, except where the block length is equal to or within 5% of the total record length of data.

The wind tunnel data presented in this paper was obtained at a test condition of Mach 0.95 and a dynamic pressure of 42 psf. The test point numbers are shown in Table 1. Additional analyses using these test points can be found in reference 16.

Table 1 Test point numbers for wind tunnel data sets

	Aileron	Tail	Aileron & Tail
Open Loop CPE	332	333	334
Closed Loop CPE	335	336	338

The control law that was active during these closed loop test points was a MIMO control law with two independent feedback loops. The horizontal tail feedback signal was derived from NIBAFTZ; the aileron feedback signal was derived from a wing inboard mid-chord accelerometer. As mentioned earlier, the results for this paper will principally show the feedback accelerometer response due to horizontal tail, HT.

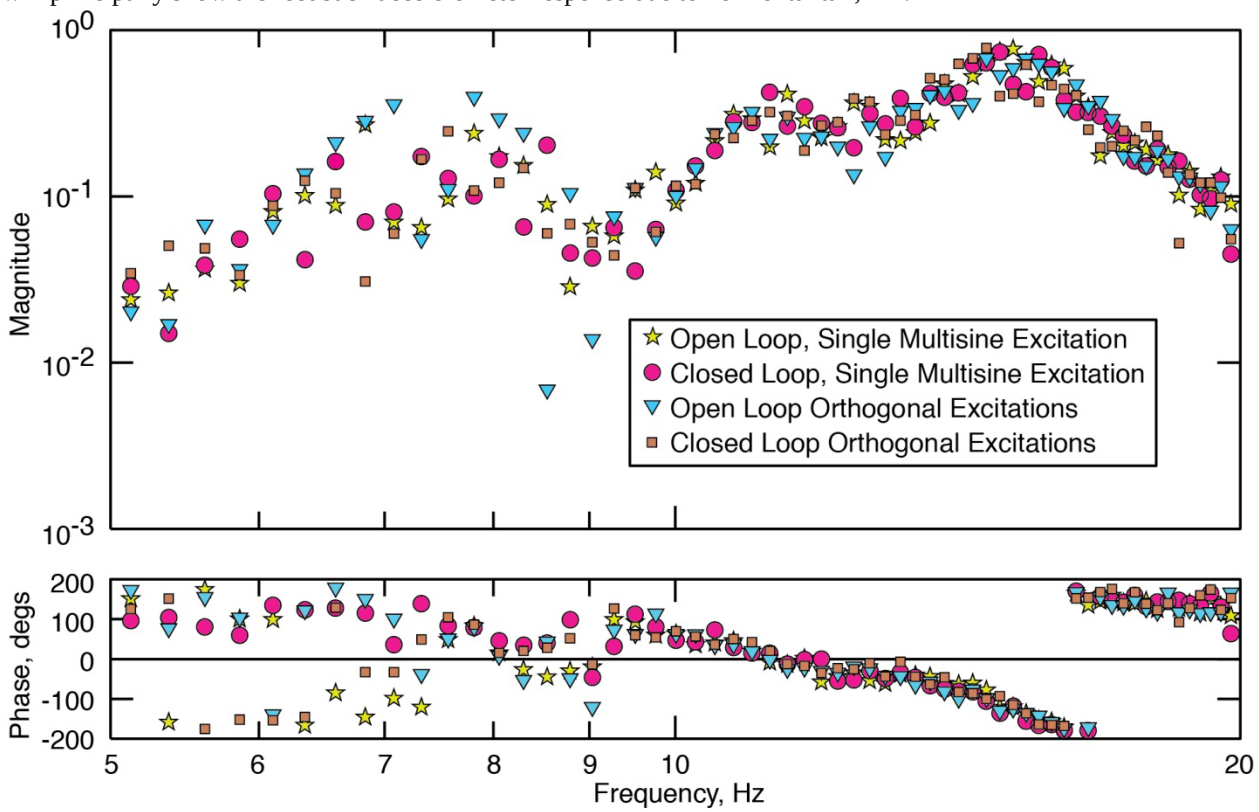

Figure 4 Frequency response functions using block size of 4096 points, 95% overlap, rectangular window; wind tunnel test data, Mach 0.95, 42 psf

Figure 4 shows magnitude and phase of the FRFs as functions of frequency. The four data sets on the plot are those that used the horizontal tail, either individually (denoted in the key as Single Multisine Excitation) or simultaneously (denoted in the key as Orthogonal Excitations). The key also indicates whether the control law was engaged (Closed Loop) or disengaged (Open Loop).

Smoothed coherence plots are shown in Figure 5. The information was smoothed for illustration purposes, as the plot of detailed coherence values at each frequency produced an illegible image. Thus, each data set was replaced

with lines showing sliding maximum and minimum values, with the maximum and minimum calculated over a range of 10 frequency points.

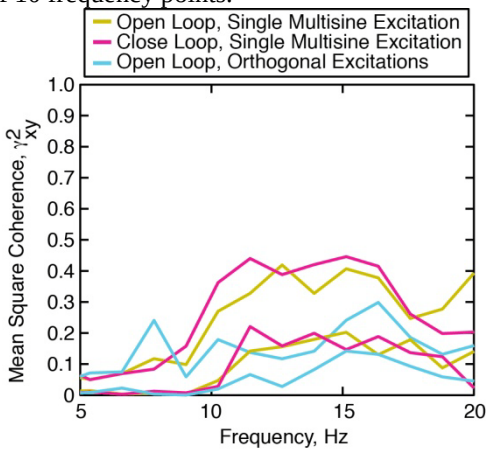

Figure 5 Smoothed coherence function 10-point maxima and minima, using Fourier block size of 4096 points, wind tunnel data at Mach 0.95, 42 psf

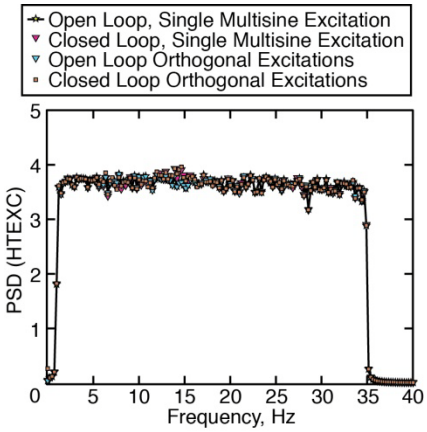

Figure 6 Power spectral density function using Fourier block size of 4096 points, wind tunnel data at Mach 0.95, 42 psf

The PSD of the excitation signal, as it was recorded by the data acquisition system, is shown in Figure 6. From the scattered results at sparse frequency points shown in the FRF, it is difficult to draw conclusions regarding the influence of open loop vs. closed loop or simultaneous excitation vs. individual excitation. Further, the low level of coherence suggests, among other possibilities, that the output is due to other inputs besides the one being considered, resolution bias errors in the spectral estimates or a nonlinear relationship between the input and output.[20] These issues are pursued using a linear simulation model.

VIII. Simulation

Multiple simulation models were developed in the S^{4}Tproject to satisfy various needs for control law development, analytical methods development and testing safety. These simulation models are documented in reference 16. For the current paper, the analytical plant and the simulated data were produced from models designated in the reference as ZEUS, with the 2010 actuator models. The following results are shown for simulation at different condition: Mach 0.8, 50 psf. The plots cannot be directly compared with the previous results shown for the wind tunnel data.

Using simulation data offers many advantages for examining the details of data processing methodology and results. Turbulence and noise can be eliminated from the data. Additionally, an analytical representation of the plant is available, providing a truth model to assess the goodness of processing changes. In the following cases, a frequency response function was generated directly from the analytical plant model at frequencies corresponding to the Fourier analysis frequencies used in processing the simulated data.

A. Processing parameter examination

Only under very special circumstances is performing a single-block Fourier analysis recommended. Bendat & Piersol, reference 20, go as far as to state *"The estimation of FRFs with two degree of freedom spectral measurements (i.e. single block processing) should never be attempted in practice. If the assumption of perfect coherence were incorrect, the FRF estimates would include severe errors… and you would have no indication (of this) from the coherence function." "Using a single block of data, the coherence function is always 1, regardless of its real coherence value."*

One of the special situations under which single block processing might be applicable is for a sinusoidal signal, whose period is exactly known and there are an integer number of samples in an integer number of full cycles being analyzed. This description corresponds to a multisine signal in a purely linear simulation, where the frequencies correspond to integer number of samples. Both the input and output information can be generated to have these characteristics. The time history data should exactly capture integer numbers of cycles and should be statistically symmetric, meaning that the first point of a cycle that appears at the beginning of the time history should not also appear at the end of the time history. Ignoring the symmetry requirement results in small leakage errors that

increase with increasing frequency. On a power spectral density plot, this will appear as a conical scatter pattern growing in diameter with increasing frequency. This characteristic will be in evidence when we return to examining the wind tunnel data. Figure 7, shows the goodness of the simulation FRF when the full time history is used in a single Fourier analysis block, obeying the above requirements.

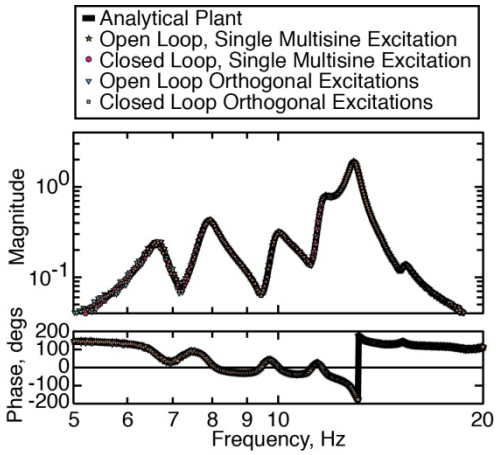

Figure 7 Frequency response functions using block size of 105000 points, simulation data, Mach 0.80, 50 psf

To examine the influence of processing parameters and examine the confidence intervals, only analysis results for the open loop single excitation results are presented.

The analysis was repeated using processing parameters typical during the wind tunnel testing to observe the difference that is generated using simulation data. Two additional choices of processing parameters sets were made. Errors in the magnitude and phase were evaluated by comparison with the analytical plant. The resulting magnitude errors are shown in Figure 8 and the phase errors are shown in Figure 9. The errors observed for the data block size of 8192 points are visibly larger than those achieved using the full time history as a single block, and larger than the errors calculated using a block size of 35000 points.

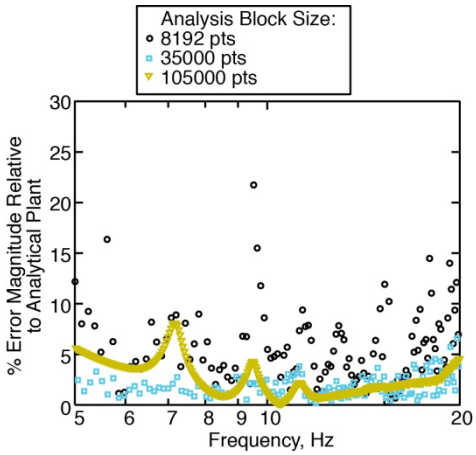

Figure 8 Error in magnitude; simulation data compared to analytical plant, Open loop, single excitation

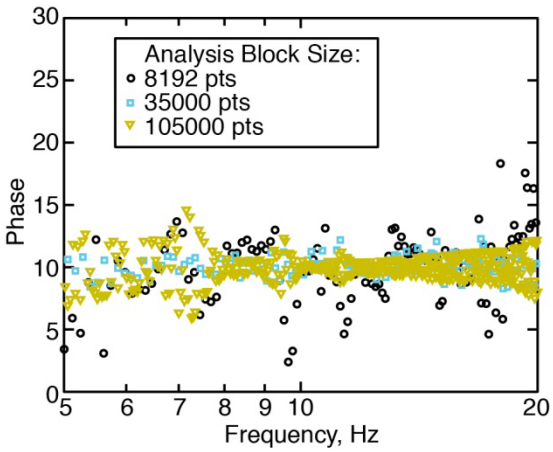

Figure 9 Error in phase; simulation data compared to analytical plant, Open loop, single excitation

The percent errors in magnitude for each case are characterized by peaks and troughs as functions of frequency. Presentation of the data in this manner can be misleading. The peaks occur at the points where the normalizing values are the lowest- at the zeroes of the FRFs. The largest errors, taken on a strict magnitude basis, correspond to the poles of the system.

The value of 35000 points was chosen because some of the Fourier analysis frequencies for this size block are frequencies present in the first multisine excitation. These intersecting frequencies are termed principal frequencies in this paper. Only those frequencies in common with a given multisine signal are preserved in analyzing this information. The values of the PSD at the other frequencies indicate the level of leakage from the multisine frequencies in-between the principal frequencies. Each multisine signal has a different set of principal frequencies. A quick glance at the PSD of a signal with the principal frequency subset chosen tells the user if they have selected the proper frequencies to correspond to a given multisine excitation. This will be shown explicitly with the wind tunnel data.

The errors shown in Figure 8 and Figure 9 indicate a substantial improvement by using the longer block size, in comparison with the 8192 points. Although the increasing block length provides some of the improvement, additional improvement is gained by the careful time history length selection. Again, this will be demonstrated using wind tunnel data.

Choices in frequency content of the multisine signals were made at the beginning of the wind tunnel test, without detailed consideration of the data processing. These choices led to the second multisine signal being composed of frequencies that cannot be exactly matched by analyzing subsets of the full time history. This is a mistake that should be corrected in future investigations. The easiest method for accomplishing this is to generate the frequencies using the desired analysis time length, which should be a subset of the total time of excitation.

B. Frequency Response Function uncertainty analysis

Using one at a time excitation, block size of 8196, the following uncertainty analyses were performed.

Two methods for assessing the frequency response function are applied here. These methods were developed by various references using an assumption of Gaussian-distributed random data, rather than sinusoidal data. The methods were also developed based on non-overlapping segments (i.e. independent data records.). Other methods were examined but not utilized in this report.[21,22,23]

1. FRF Method 1:

The confidence intervals or standard deviations of the magnitude and phase of the FRFs can be estimated using the coherence and FRF estimates, which are generated using a given number of data sets. For the S^4T analysis case, each overlapped average segment is treated as a separate data set. The data analysis in reference 24 assumed that the influence of bias errors had been minimized, and the primary source of error was random error arising from unmeasured excitations. The magnitude and phase values at each given frequency were assumed to be Gaussian-distributed random variables.

Error bounds on the FRF estimates are calculated here, following the method given in reference 24, using Eqs (4) and (5). Results produced from this method are denoted FRF Method 1.

$$\hat{\sigma}(|\hat{G}(\omega)|) = \frac{\sqrt{1-\hat{\gamma}_{xy}^2(\omega)}}{|\hat{\gamma}_{xy}|\sqrt{2}}|\hat{G}(\omega)| \tag{4}$$

$$\hat{\sigma}(angle(\hat{G}(\omega)) = sin^{-1}\left(\frac{\sqrt{1-\hat{\gamma}_{xy}^2(\omega)}}{|\hat{\gamma}_{xy}|\sqrt{2}}\right) \tag{5}$$

The upper and lower bounds on the magnitude and phase were calculated using 3σ limits, shown in Figure 10.

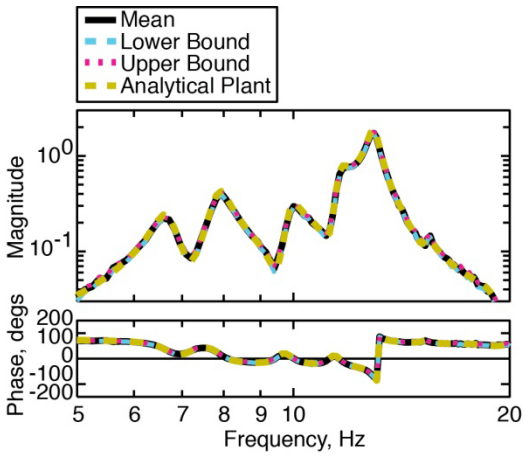

Figure 10 FRF Method 1 of calculating uncertainty bounds; open loop single excitation of simulation model; 8192 points in Fourier analysis block

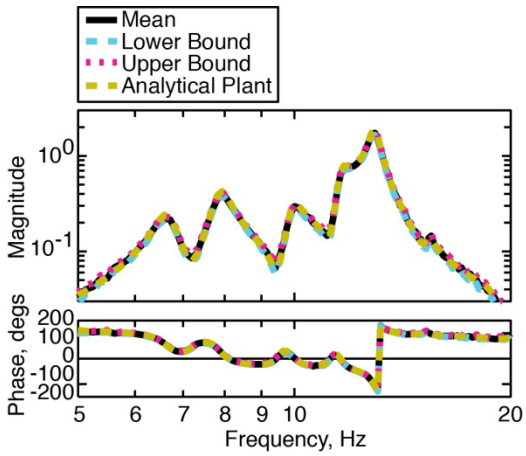

Figure 11 FRF Method 2 of calculating uncertainty bounds; open loop single excitation of simulation model; 8192 points in Fourier analysis block

2. FRF Method 2

A second method to assess the uncertainties of the FRF- denoted FRF Method 2- is applied, following the process outlined in reference 20. This method accounts for random error in the measured FRF. Specified in the reference by eqn 6.146, and reproduced here in Eqns (6) and (7), a confidence interval with confidence 100*(1-α)% can be calculated. Equation (6) says that the difference between the estimated plant and the true plant is less than the bound given by (7). From (7), the error in FRFs is dependent on the degrees of freedom and the coherence. The uncertainty in the calculation decreases as the number of ensembles, n, used in the averaging for computing the spectral estimates increases or as the coherence increases towards 1.

$$|\widehat{G}(f) - G(f)|^2 \leq \hat{r}(f)^2 \tag{6}$$

$$\hat{r}(f) = \frac{2}{(n-2)} F_{2,n-2,\alpha}[1 - \hat{\gamma}_{xy}^2(f)] \frac{\hat{P}_{yy}}{\hat{P}_{xx}} \tag{7}$$

The S^{4}T simulation data, with 105 seconds in the time history, with 8192 points in the analysis block size, with 95% overlap has 237 overlapped analysis segments. The associated value of the F-distribution, $F_{2,235,0.05} = 3.03392$. Results from applying FRF Method 2 are shown in Figure 11. The uncertainty bounds are almost identical to those produced by FRF Method 1. There are small changes in the bounds near the zeros- valleys- of the FRFs.

The same analyses are performed using the simulation data with simultaneous excitations. The results of applying method 1 are shown in Figure 12; the results of applying method 2 are shown in Figure 13. In the case of simultaneous excitations, the coherence functions are lower, leading to larger confidence intervals on the FRFs, as compared to those calculated for the single excitation data, Figure 10 and Figure 11. Comparison of the results from the two methods shows that, although each method is applied to generate confidence intervals of 95%, the answers obtained are noticeably different. Larger uncertainty regions are found using the second method. No attempt was made to duplicate the derivations of either work to determine the point at which the methods diverge, or the difference in underlying assumptions.

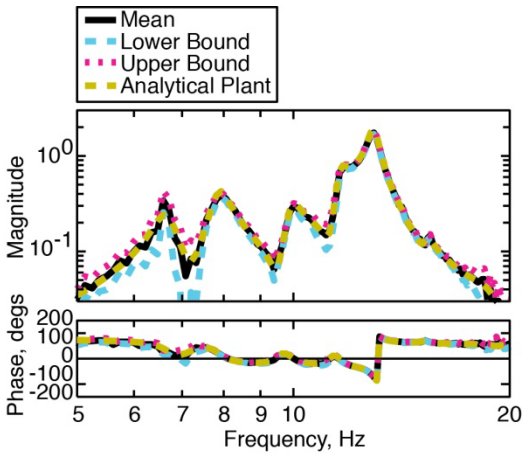

Figure 12 FRF Method 1 of calculating uncertainty bounds; open loop simultaneous excitation of simulation model; 8192 points in Fourier analysis block

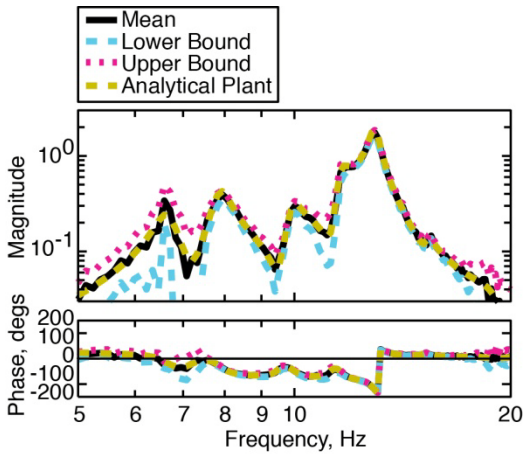

Figure 13 FRF Method 2 of calculating uncertainty bounds; open loop simultaneous excitation of simulation model; 8192 points in Fourier analysis block

C. Coherence uncertainty analysis

Both of the described methods for estimating the uncertainty bounds on the FRF rely on calculation of the coherence function, which itself contains uncertainty. In the above calculations of the uncertainty bounds, the coherence functions computed from the ensemble means of the cross spectral density and power spectral density functions were used. The uncertainties on the coherence function were assessed using 2 methods. Other methods were found in the literature, reference 25 for example. However, none of these methods appeared any more applicable to sinusoidal data than the two applied below.

The first method, from Bendat & Piersol[20] and utilized by Bortel & Sobka,[26] requires that the segments be non-overlapping. This method, denoted here as Coherence Method 1, is an approximate method, developed based on random Gaussian process assumptions, that has been demonstrated to be valid for coherence values between 0.35 and 0.95 when greater than 20 segments are used in the ensemble averages, according to references cited. The method was applied, regardless of the restriction in the development pertaining to independent segments and Gaussian processes. The approximate equations used in the calculation include evaluation of the standardized normal distribution at the 100α point, and specify the (1-α)*100 % confidence bounds.

The open loop single excitation data was first analyzed. The coherence and the 95% confidence bounds calculated using Method 1 are shown in Figure 14.

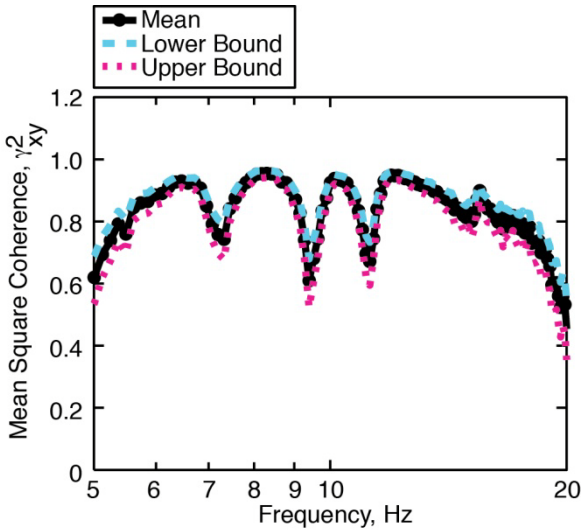

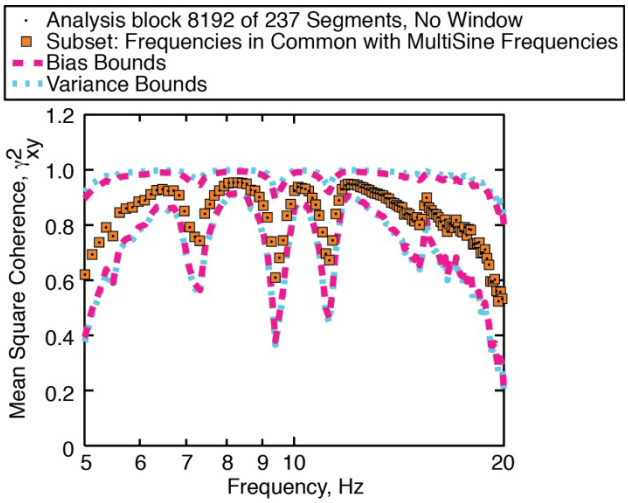

Figure 15 Coherence Method 2 for calculating uncertainty

Figure 14 Coherence Method 1 for calculating uncertainty bounds, open loop single excitation, block size of 8192 points

The second method, presented by Carter, Nutall & Knapp,[27] and utilized (or perhaps developed independently) by Touzi etal[28], was also developed with the assumptions of non-overlapping data segments and Gaussian distributed data. The equations of reference 27, not reproduced here, provide assessments of the bias and variance of the coherence function. The computations involve evaluations of a hyper geometric series.[29] These evaluations are accomplished using software cited as reference 30. The results of applying this method are shown in Figure 15. It is unclear how the uncertainties should be combined to form an overall uncertainty estimate. Thus, they are left as individual components as indicated in the figure. This method is denoted here as Coherence Method 2.

The same analyses are performed using the simulation data with simultaneous excitations. Coherence Method 1 results are shown in Figure 16 and Coherence Method 2 results are shown in Figure 17. Again, Coherence Method 2 produces larger uncertainty regions than Coherence Method 1.

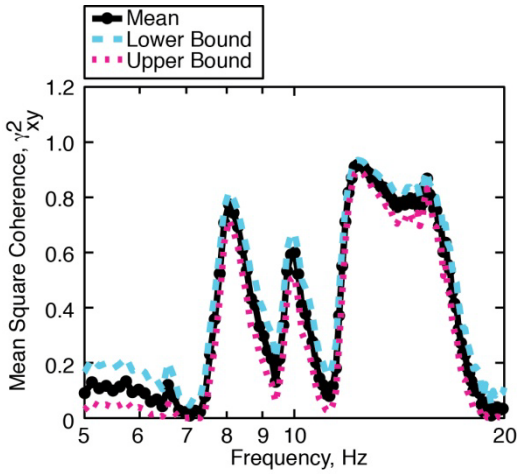

Figure 16 Coherence Method 1 for calculating uncertainty bounds, open loop simultaneous excitation, block size of 8192 points

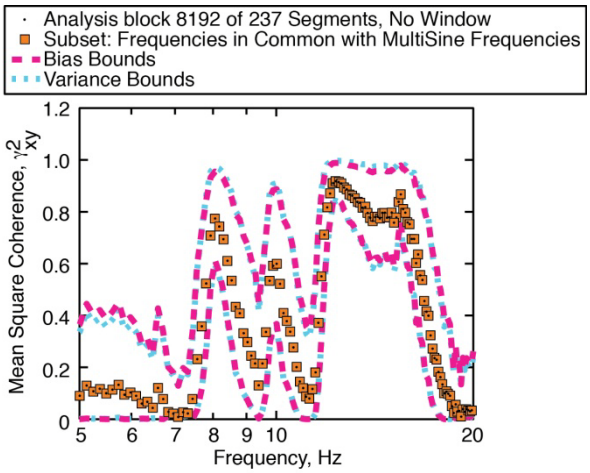

Figure 17 Coherence Method 2 for calculating uncertainty bounds, open loop simultaneous excitation, block size of 8192 points

D. Coherence characteristics

In the previous results, there was a qualitative difference between the individual excitation coherence, Figure 14 Figure 15), and the simultaneous excitation coherence, (Figure 16Figure 17). Figure 18 shows the coherence of both the horizontal tail and aileron, actuated one at a time. The coherence for a single excitation is high throughout the frequency range for both excitations. The dips in these coherence traces correspond to zeros of the FRFs, and are likely the result of insufficient frequency resolution in regions where the characteristics change sharply with frequency. The coherence functions for the simultaneous excitations, shown in Figure 19, are poor for each surface over different portions of the frequency range. The coherence associated with a given control surface is high when the matching FRF's magnitude, Figure 20, is dominantly larger than the other control surface's FRF magnitude.

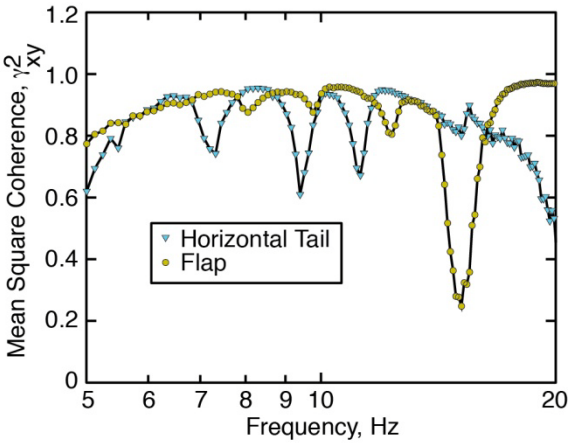

Figure 18 Coherence due to each control surface, actuated individually, open loop, 8192 points

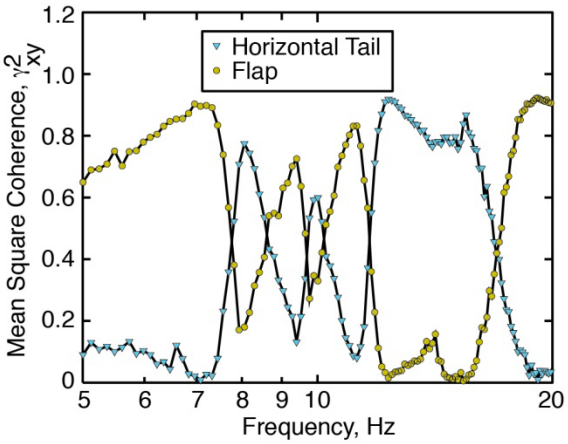

Figure 19 Coherence due to each control surface, actuated simultaneously, open loop, 8192 points

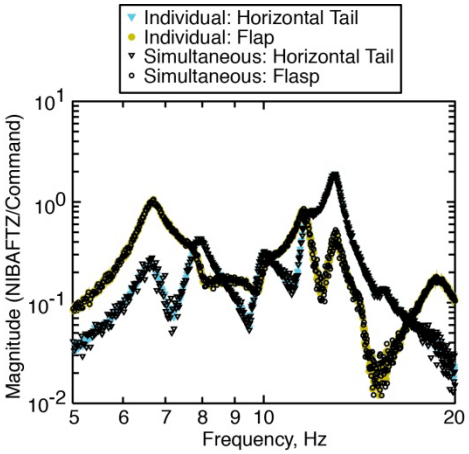

Figure 20 Frequency response functions, actuated individually & simultaneously, open loop, 8192 points

The frequency response functions shown in Figure 20 appear nearly identical, regardless of whether the inputs are individual or simultaneous. The coherence plots, however, seem to indicate that these simultaneous inputs cannot be treated as orthogonal. The possible explanations include misinterpretation of the results shown, mistakes in data processing, mistakes in setup or conduct of the experiment, or misapplication of the underlying theory. The issue requires further scrutiny before proceeding with more detailed analysis of the simultaneous actuation cases. This will be addressed in future work.

IX. Wind tunnel data, Revisited

The wind tunnel data is now reanalyzed considering the trends observed through simulation data.

A. Time stretching of input signals

In the initial processing of the wind tunnel data, it was assumed that the time length of the excitation was exactly as it had been generated in software- time length 105 seconds, sampled at 1000 samp/sec producing105000 samples. Examination of the signal recorded during testing by the data acquisition system, Figure 21, reveals that the signal was stretched adding 3 samples to the record length required to complete the excitation. To see this from the figure, examine first the initial time points selected in the left-hand zoom box; in the figure, points selected as belonging to the excitation are shown by the yellow encirclements. The first point selected is the last zero value at the beginning

of the time history. Recalling statistical symmetry, the last point in the selected time history should be the last non-zero point of the excitation. Examining the right-hand zoom box, the last point selected, point number 105000, is approximately 3 points shy of completing the excitation. An argument could be made that it is closer to 4 points shy of completing the excitation. Frequency domain analysis will clarify the best integer number of samples to select, in light of this implementation issue.

This signal stretching means that the frequencies present in the signals as they were implemented contained lower frequencies than those of the designed multisine signals. With random excitation and data reduction methods, the effect of stretching a random signal would not be noticeable or likely important. In trying to carefully preserve the multisine signals' complete cycles, these points are now included. The source of the signal stretching has not been identified, but has been shown to be present in both the JWS test data and the S^4T test data. Identical hardware and software was utilized in these two tests, although excitation signal definition was performed independently and at different sample rates.

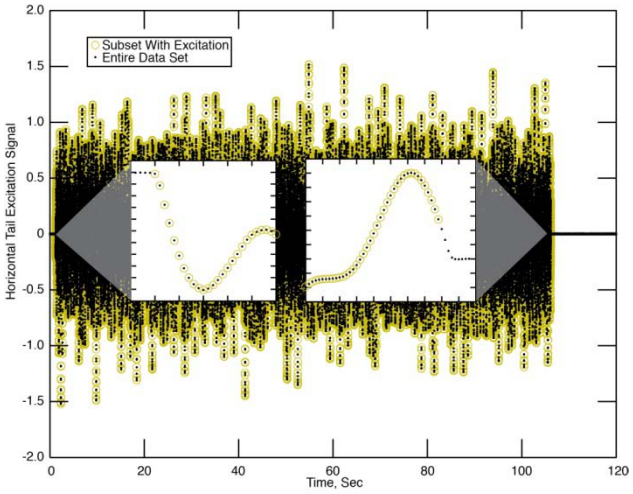

Figure 21 Time history of excitation signal showing end point mismatch

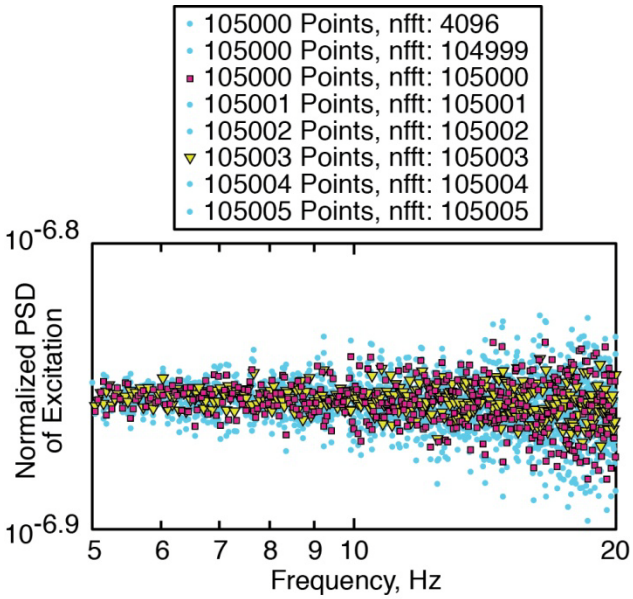

Figure 22 Normalized power spectral density function of horizontal tail excitation, wind tunnel data

It was previously discussed that the truncation of a single point from the time history leads to incomplete cycles in the excitation. The multisine signals are designed such that they return to a zero value at the end of the excitation sequence. Truncating the last few points produces a discontinuity and introduces broad-spectrum leakage into the analysis.

Because the time history is stretched and the frequencies each lowered, there is also a mismatch between the frequency content of the signal and the frequencies of a Fourier analysis. As frequency increases, the offset between the signal content and the analysis frequencies increases. The leakage effect thus increases as the frequency increases- indicated in Figure 22 by the conical scatter pattern of the results. The scatter in the plot is due to the random phase angle that has been assigned to each of the multisine components.

The variation is minimized by selecting the block length to be 105003 points, corresponding to a time length of 105.003 seconds. It is again emphasized that a single block analysis is seldom a good choice. Detailed study of the PSD can serve as a warning sign that the processing parameters need to be adjusted.

The scatter pattern here emphasizes that the time length required to capture the excitation needs to increase to 105003 points. Although the information was presented in reverse order, the issue with the time stretching was discovered in investigating the source of the scatter on the PSD plot. The stretching of the excitation results in a reduction of all of the frequencies in the multisine excitation signal as it was implemented during the test. In performing additional analyses on the wind tunnel data, a new set of frequencies approximating the implemented frequencies is used. This inexact match makes all of the wind tunnel results less pristine than might otherwise be expected.

B. Leakage effects

As pointed out by Schoukens, Rolain and Pentelon in reference 31:
"Measuring a periodic signal over an integer number periods removes the leakage problem completely, and we strongly advise the reader to apply periodic excitation signals whenever it is possible."
Implementation issues have prevented this from being achieved, although it is still a worthy goal for future testing.

Paralleling the choices evaluated in simulation, a subset of the data is again chosen as 1/3 of the total time length record. The power spectral density plot, showing some of the implications of this choice for test data, is illustrated in Figure 23. The PSDs are again normalized so that the results from different block lengths can be directly compared. The result for block size 105003 from above is repeated for reference. The reduced block size results are shown by the grey dots.

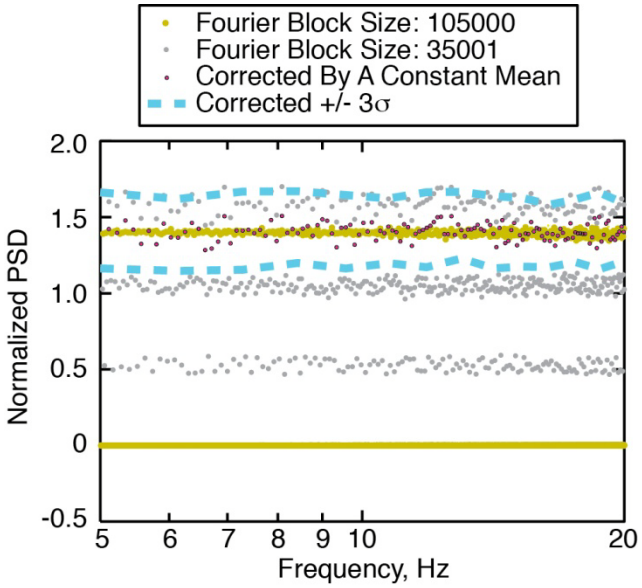

Figure 23 Normalized power spectral density function of horizontal tail excitation, wind tunnel data

Notice the strata that are formed. There are 4 strata, with the middle 2 overlapping and becoming indistinguishable on this plot. The upper highest stratum comes from the data points where the frequencies align with the near-multisine frequencies. The lowest stratum comes from those frequencies that align with the other multisine signal in this 2-orthogonal-signal data set. The other two sets combine together in the center strata and arise from the points that are stepped over by the multisine signal generation process. Where the frequency does not align with an excitation frequency component of the multisine, the amplitude is lower than at the excitation frequencies.

Notice that the effect of leakage is actually to increase the value of the PSD at the multisine frequencies. This is because these frequencies have full energy from 1 multisine component, plus the leakage contributions of all of the non-principal frequencies.

The PSD can be corrected to eliminate the leakage effect- it can be done based on analytical expressions derived from Parseval's theorem if the frequencies are exactly known. For a pristine multisine signal with a uniform distribution, the power spectral density function is ideally zero at non-excitation frequencies, and a constant value at the excitation frequencies. The value of the PSD can be calculated using (8), where K and n_f are as discussed in (2).

$$PSD(f_{MS}) = \left(K * \sqrt{\frac{1}{n_f}} \right)^2 * \frac{nfft}{2 * samp} \tag{8}$$

In the PSD normalizations shown in this paper, they are divided by nfft so that different block sizes can be compared. The S^4T wind tunnel test data presented in this paper had the test-settable factor, K, set to ½. Thus, the anticipated value of the normalized PSD is (1/2)^2 * (1/893)/(2*1000) = 1.40e-7. Including only the principal frequencies in the computation of the mean, shown by the yellow dots in Figure 23, the mean value of the normalized PSD data with a single 105003 block size is 1.3886e-7.

The variation bounds shown on the plot correspond to analysis of the measured data, which produces a non-pristine signal, as discussed previously.

The leakage effects shown here are the "interpolation error due to the combination of neighboring spectral lines," discussed by Schoukens, Rolain and Pentelon.[31]

Using a rectangular window has its drawbacks, and one of them is leakage when the frequencies are not exactly windowed by the time length. From Bendat & Piersol, 1980[32], *"… the large side lobes of (the the frequency domain representation of the window) allow leakage of power at frequencies well separated from the main lobe of the spectral window and may introduce significant anomalies in the estimated spectra, particularly when the data are sinusoidal…"* This has been demonstrated to be the case in the analysis of these multisine data sets.

C. Analysis with the chosen processing parameters

Frequency response function estimates are computed and shown in Figure 24 for the same cases as originally shown in Figure 4, but using the newly selected block length and frequency downselection process. The frequency resolution has improved by virtue of the extended block size, as indicated by the denser spacing of points for all data sets.

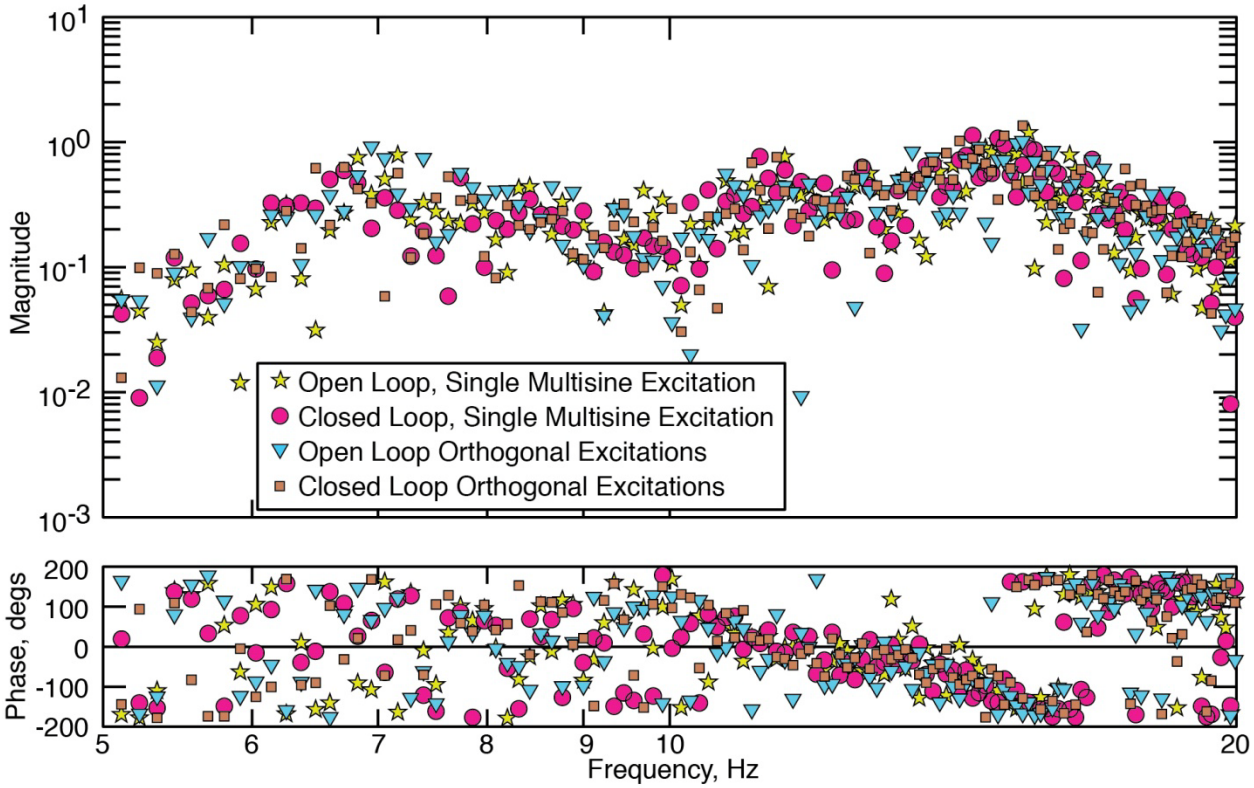

Figure 24 Frequency response functions using block size of 35001 points, wind tunnel test data, Mach 0.95, 42 psf

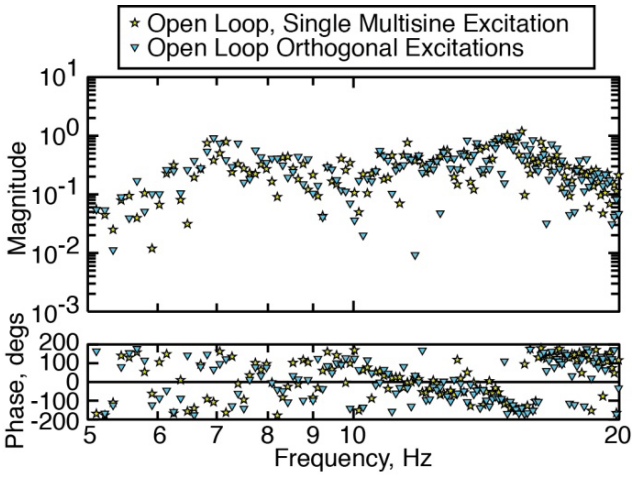

Figure 25 Frequency response functions using block size of 35001 points, wind tunnel test data, Mach 0.95, 42 psf

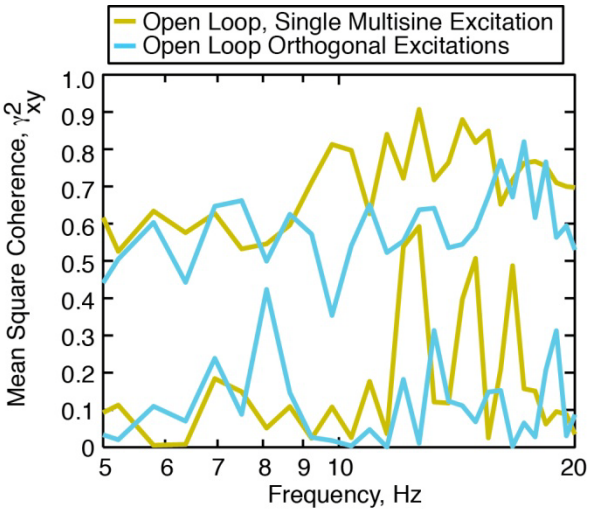

Figure 26 Coherence maxima and minima, using block size of 35001 points, wind tunnel test data, Mach 0.95, 42 psf,

These improvements can be demonstrated to be at least partially due to selection of the frequencies aligning with the multisine frequencies, rather than only due to increased block size. Comparison with a window that is slightly longer, 36000 samples, yields a qualitatively worse FRF,
Figure 27, and a quantitatively degraded coherence plot, Figure 28.

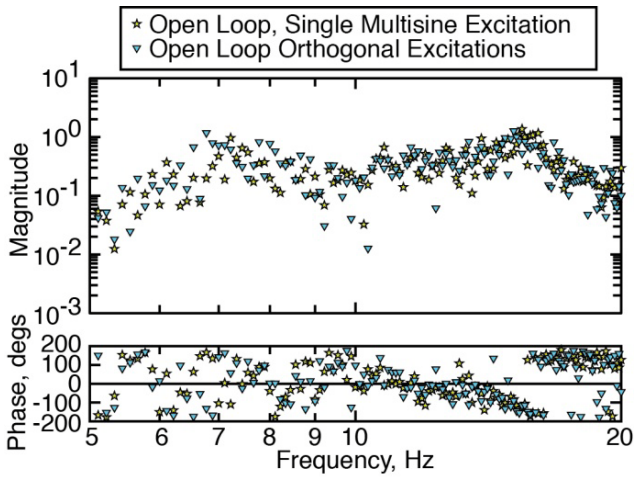

Figure 27 Frequency response functions using block size of 36000 points, wind tunnel test data, Mach 0.95, 42 psf

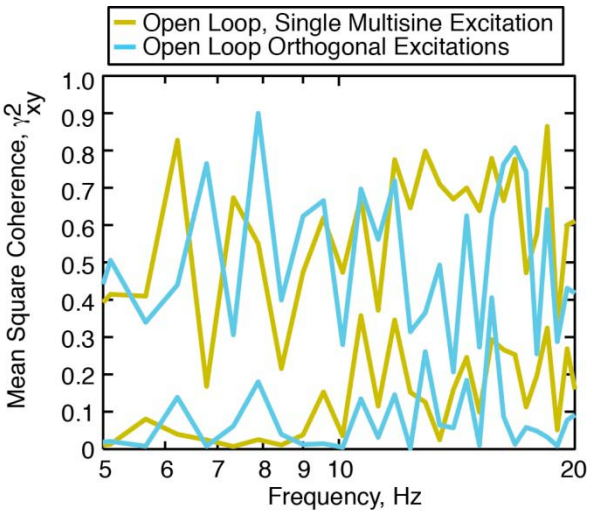

Figure 28 Coherence maxima and minima, using block size of 36000 points, wind tunnel test data, Mach 0.95, 42 psf

\

D. Assessment of improvements

In a final assessment, the results from the revised processing are compared with the original processing for the open loop single excitation case. The results from processing with a single block are shown on the plots for reference. The FRF, Figure 29, is clearly modified from the original processing parameters. Without a truth model, it still remains difficult to assess whether or not the estimated function is an improvement over the original version. The coherence function, Figure 30, appears vastly improved relative to the original version. This indicates that the revised FRF is a better representation of the linear relationship between the input and the output, and implies reduced uncertainty on the FRF calculation when the longer, frequency-crafted segment length is used. A histogram of the coherence results, provided in Figure 31, shows that the FRF is generally improved by the reprocessing.

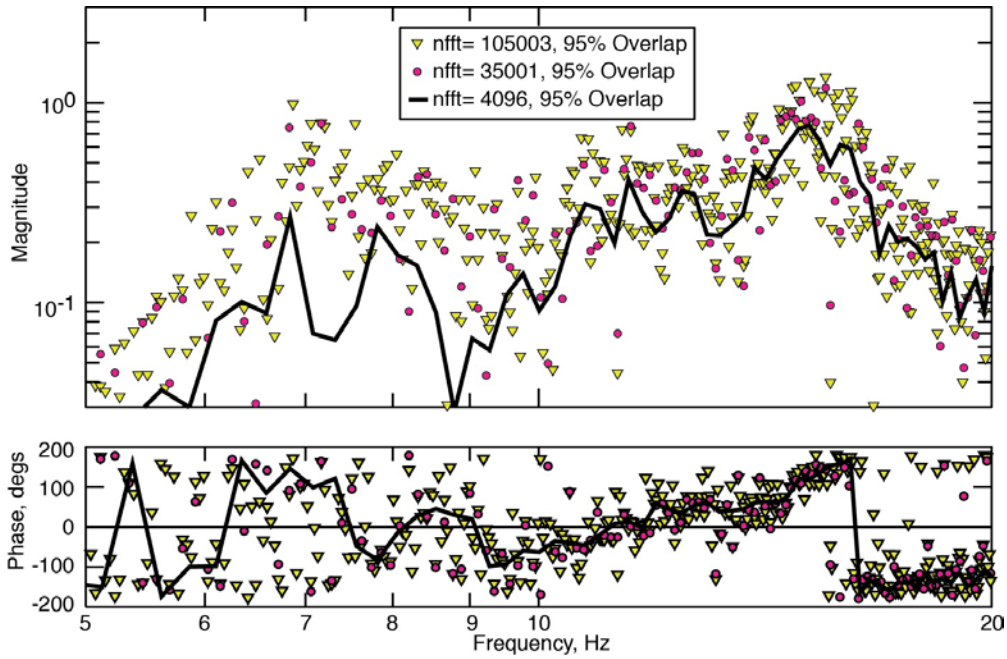

Figure 29 Frequency response functions, comparison of using block sizes, wind tunnel test data, Mach 0.95, 42 psf

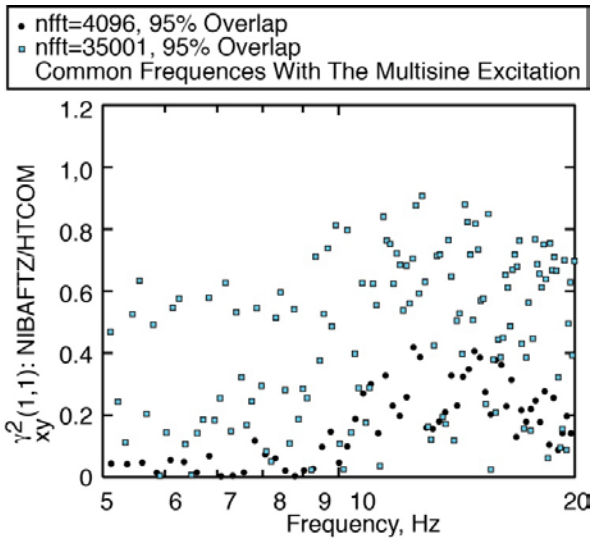

Figure 30 Coherence, comparison of using block sizes, wind tunnel test data, Mach 0.95, 42 psf

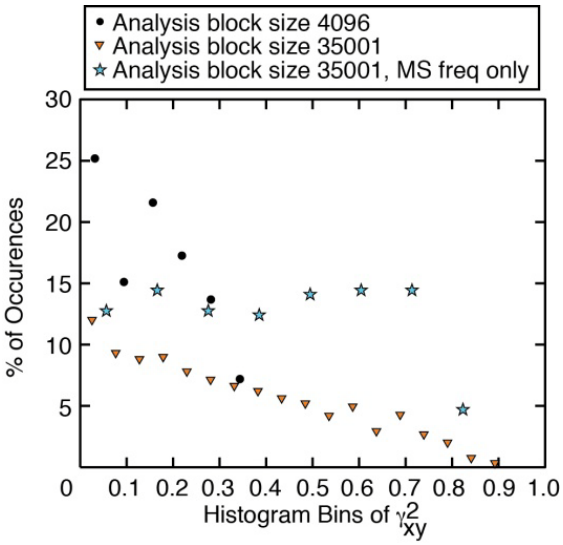

Figure 31 Histogram of coherence, comparison of using block sizes, wind tunnel test data, Mach 0.95, 42 psf

X. Concluding remarks

The potential advantages of matching the processing frequencies to the excitation frequencies were demonstrated through simulation and through wind tunnel data. Implementation issues corrupted the wind tunnel data in such a way that adjustments had to be made to the frequencies, rather than using the original generated and thought-to-be-applied frequencies. Attempts were made to compensate for this slight mismatch, but it remains the source of some variation in the results. Additionally, the frequency selection algorithm should be modified to allow subsets of the time history to be used to produce frequency response function estimates.

With regard to the simultaneous orthogonal excitations, much work remains to be done. The coherences and frequency response functions indicate that the uncertainty assessment using ordinary coherence functions is likely not applicable. Further, the methods used for assessing the uncertainty are based on Gaussian distribution assumptions, rather than a distribution that is perhaps more suitable to sinusoidal data.

XI. Future work & Recommendations

The fundamental objective of the continued work applying multisine excitations is to develop and apply a set of excitations that allow simultaneous system identification of a multiple control effector system. This involves finding a methodology for decorrelating the command signals for a system that has decorrelated excitations. Corrupting process include the usual culprits in producing bias and variance in the data, including natural turbulence introduced by the wind tunnel airstream, control surface interference effects- both structural and aerodynamic- and unknown noise sources. The current work and the previous publication analyzing data from the Joined Wing Sensorcraft begin to approach these issues, but require further development and experience. Specific issues for future investigation include the following.

1) Apply expressions for uncertainties of the FRF and coherence based on sinusoidal assumptions rather than on Gaussian random data assumptions.
2) In the cases where the assumption has been made that the segments are non-overlapping, apply and/or develop the expressions for overlapping segments.
3) Determine the source of time stretching in the data generation and acquisition processing in the experimental test set-up
4) Investigate the advantages of extending the data record in simulation to include a significant number additional time points relative to the record length used to generate the multisine signals. Apply

approximate methods that involve upsampling and splining of the results, such that the methods for handling multisine results are accessible and easy for practitioners.

5) Apply these same general methods to analysis of short time records pertinent to unsteady computational fluid dynamic simulation results.
6) Investigate harmonic distortion through simulation results and analytical methods
7) Investigate methods for properly representing and combining sources of uncertainty

In future applications of the multisine orthogonal excitation method, the following recommendations are made.

Through analysis of the data shown, analysis and derivations involving sinusoidal excitations and considerable literature absorption, the following recommendations are made regarding applying multisine excitations for aeroelastic system identification.

Conduct a simulation of the experiment ahead of time, including data reduction. Simulation will help eliminate mis-steps in signal generation, application and processing.

Choose the time length of the signal generating window (which will later match your ensemble length) to analyze based on the desired resolution.

Formulate the multisine functions to have a shorter time length to complete a whole multisine excitation period than the total excitation window length. Alternately, generate the excitation time histories to extend beyond their original signal generation time window. Utilize this data to evaluate the practicality of the methods shown in reference.[10]

For analyzing multisine data, it is recommended that the signal be designed such that entire cycles can be fit into an analysis window, and analyzed as a full cycle.

XII. References

[1] Morelli, E.A. "Flight-test experiment design for characterizing stability and control of hypersonic vehicles," *Journal of Guidance, Control, and Dynamics*, Vol. 32, No. 3, May-June 2009, pp. 949-959.

[2] Heeg, J. and Morelli, E., Evaluation of simultaneous multisine excitation of the Joined Wing SensorCraft aeroelastic wind tunnel model, 52nd AIAA/ASME/ASCE/AHS/ASC Structures, Structural Dynamics and Materials Conference, Denver Colorado, April 2011.

[3] Martinez, J., "An overview of SensorCraft capabilities and key enabling technologies," 26th AIAA Applied Aerodynamics Conference, No. AIAA-2008-7185, Honolulu, Hawaii, August 2008.

[4] Reichenbach, E., "Aeroservoelastic design and test validation of Joined Wing SensorCraft," 26th AIAA Applied Aerodynamics Conference, No. AIAA-2008-7189, Honolulu, Hawaii, August, 2008.

[5] Scott, M., "SensorCraft free-flying aeroservoelastic model design and fabrication," 52nd AIAA/ASME/ASCEAHS/ASC Structures, Structural Dynamics and Materials Conference, Denver Colorado, April 2011.

[6] Hoagg, J.B., Lacy, S.L, BabuˇskaV, and Bernstein, D.S., "Sequential multisine excitation signals for system identification of large space structures," proceedings of the 2006 American Control Conference, Minneapolis, Minnesota, USA, June 14-16, 2006.

[7] Perry, Boyd, et al., "Plans and status of wind-tunnel testing employing an aeroservoelastic semispan model," 48th AIAA/ASME/ASCEAHS/ASC Structures, Structural Dynamics and Materials Conference, No. AIAA-2007-1770, Honolulu, Hawaii, April 2007.

[8] Florance, J. R; Silva, W. A; Perry, B, III; Sanetrik M D.; Scott, R.C.; Keller, D.F; Design, Fabrication and Characterization of the SemiSpan Supersonic Transport (S4T) Wind-Tunnel Model, AIAA paper submitted to 53rd SDM Conference.

[9] Christhilf, David, Pototzky, Anthony S., and Stevens, William, "Incorporation of SemiSpan SuperSonic Transport (S4T) aeroservoelastic models into SAREC-ASV simulation", AIAA Modeling and Simulation Technologies conference, AIAA-2010-8099, Toronto, Ontario, August 2010.

[10] Schoukens, J., Rolain, Y, Simon, G, and Pintelon, R., "Fully automated spectral analysis of periodic signals," IEEE Transactions on instrumentation and measurement, Vol. 52, No. 4, August 2003.

[11] Oppenheim, Alan V. and Schafer, Ronald W., Discrete-time signal processing, 1989, Prentice-Hall, Inc, Englewood Cliffs, New Jersey

[12] Hardin, Jay C., Introduction to time series analysis, NASA Reference Publication 1145, Nov 1990.

[13] Pototzky, Anthony S., Wieseman, Carol D., Hoadley, Sherwood T., and Mukhopadhyay, Vivek, "Development and testing of methodology for evaluating the performance of multi-input/multi-output digital control systems," NASA TM-102704, Aug 1990.

[14] Wieseman, C.D., Hoadley, S.T. and McGraw, S.M., On-line analysis capabilities developed to support the AFW Wind-tunnel tests, NASA TM 107651, July 1992.

[15] Pototzky, A.S., Wieseman, C.D., Hoadley S.T. and Mukhopadyay, Vivek Carol Wieseman, Sherwood Tiffany Hoadley and Vivek Mukhopadhyay, On-Line Performance Evaluation of Multiloop Digital Control Systems , Journal of Guidance, Control and Dynamics, Vol. 15, No. 4, July-August 1992

[16] Wieseman, C.D., and Christhilf, D., Analytical and experimental evaluation of digital control systems for the semi-span super-sonic transport (S4T) project, AIAA paper submitted to 53rd SDM Conference.

[17] Harris, F.J., "On the use of windows for harmonic analysis with the discrete Fourier transform," Proceedings of the IEEE, Vol 66, No 1, January 1978.

[18] Antoni, J., and Schoukens, J, "Optimal settings for measuring frequency response functions with weighted overlapped segment averaging," IEEE transactions on instrumentation and measurement, Vol 58, No 9, Sept 2009.

[19] Widanage, W.D., Douce, J.L, and Godfrey, K.R., "Effects of overlapping and windowing on frequency response function estimates of systems with random inputs," IEEE Transactions on instrumentation and measurement, Vol 58, No 1, January 2009.

[20] Bendat, J.S., and Piersol, A.G., "Random data: Analysis and measurement procedures," John Wiley & Sons, Inc, New York, 1971.

[21] Douce, J.L, and Balmer, L, "Statistics of frequency response estimates," IEE Proceedings, Vol 137, Pt D, No 5, September 1990.

[22] Fornies-Marquina, J.M., Letosa, J. Garcia-Gracia, M, and Artacho, J.M, "Error propagation for the transformation of time domain into frequency domain," IEEE Transactions on Magnetics, Vol 33, No 2, March 1997.

[23] Douce, J.L., Widanage, W.D, and Godfrey, K.R., "Errors in frequency response estimates using overlapping blocks with random inputs," 15th IFAC Symposium on system identification, Saint-Malo, France, July 6-8, 2009.

[24] Doebling, S.W., and Farrar, C.R., Estimation of statistical distributions for modal parameters identified from averaged frequency response function data, Los Alamos National Laboratory, LA-UR-00-41, July 2000.

[25] Wang, S.Y., and Tang, M.X., "Exact confidence interval for magnitude-squared coherence estimates," IEEE signal processing letters, Vol 11, No 3, March 2004.

[26] Bortel, R., and Sovka, P., "Approximation of statistical distribution of magnitude squared coherence estimated with segment overlapping," Signal Processing 87 (2007) 1100-1117.

[27] Carter, G.C, Knapp, C.H., and Nuttall, A.H, "Statistics of the estimate of the magnitude-coherence function," IEEE transactions on audio and electroacoustics, August 1973.

[28] Touzi, Ridha, Lopes Armand, Bruniquel, J., and Vachon, P.W., "Coherence estimation for SAR imagery," IEEE Transactions on geosciences and remote sensing, Vol 37, No 1, January 1999.

[29] Evans, M., Hastings, N, and Peacock, B., "Statistical Distributions," 3rd edition, John Wiley & Sons, Inc, New York, 2000.

[30] Perger, W.F., Nardin, M., Bhalla, A., Michigan Technology University, 1993; Translated by Barrowes, B.E., MIT, July 2004.

[31] Schoukens, J., Rolain, Y., and Pentelon, R, "Analysis of windowing/leakage effects in frequency response function measurements," Automatica 42 (2006) P 27-38.

[32] Bendat, J.S., and Piersol, A.G., "Engineering applications of correlation and spectral analysis," John Wiley & Sons, New York, 1980.